Eur. Phys. J. A **6**, 175–183 (1999)

THE EUROPEAN PHYSICAL JOURNAL A

Excited Superdeformed Band in ^{143}Eu

A. Axelsson[1], J. Nyberg[2], A. Ataç[1,2], M.H. Bergström[3], B. Herskind[3], G. de Angelis[4], T. Bäck[5], D. Bazzacco[6], A. Bracco[7], F. Camera[7], B. Cederwall[5], C. Fahlander[4a], J.H. Huijnen[2], S. Lunardi[6], B. Million[7], D.R. Napoli[4], J. Persson[1], M. Piiparinen[8], C. Rossi Alvarez[6], G. Sletten[3], P.G. Varmette[3], M. Weiszflog[2]

[1] Department of Radiation Sciences, Uppsala University, Uppsala, Sweden
[2] The Svedberg Laboratory, Uppsala University, Uppsala, Sweden
[3] The Niels Bohr Institute, University of Copenhagen, Copenhagen, Denmark
[4] INFN, Laboratori Nazionali di Legnaro, Legnaro, Italy
[5] Royal Institute of Technology, Stockholm, Sweden
[6] Department of Physics, University of Padova and INFN Padova, Padova, Italy
[7] Department of Physics, University of Milano and INFN Milano, Milano, Italy
[8] Department of Physics, University of Jyväskylä, Jyväskylä, Finland

Received: 5 July 1999
Communicated by B. Povh

Abstract. A new superdeformed band has been discovered in a EUROBALL experiment and assigned to ^{143}Eu. It has a maximum intensity of 35% of the ^{143}Eu yrast superdeformed band and the transition energies of the two bands are very similar. Based on comparison with cranked shell model calculations the new band is tentatively assigned the high-N intruder configuration $\pi 6^2 \nu 7^0$ and the parity and signature quantum numbers $(\pi, \alpha) = (-1, +1/2)$. In addition to the already known high-energy transition at 3361 keV another discrete line at 2715 keV was found to be in coincidence with the yrast superdeformed band. However, it was not possible to connect the decay out of either of the superdeformed bands to known normally deformed states.

1 Introduction

It has been predicted by fluctuation analysis that there are ∼30–40 discrete bands in the superdeformed (SD) well of ^{143}Eu [1]. The intensity of the discrete transitions compared to the intensity of the superdeformed ridge structure in the feeding energy region suggests that several of these excited bands should be well within the observation limits of the large arrays currently in use. The first such excited superdeformed band in ^{143}Eu has now been identified, with a maximum intensity of 35% compared with the yrast superdeformed band. The new band reveals a spectrum almost identical to that of the yrast band over ∼10 transitions, but decays out at a rotational frequency almost twice as high.

2 Experiment and data reduction

The experiment was performed with the EUROBALL γ-ray spectrometer [2] during the first phase of operation at the Legnaro National Laboratory. EUROBALL consists of a total of 239 HPGe detectors in an arrangement of 15 cluster detectors, each consisting of seven large-volume crystals sharing a single BGO Compton-suppression shield, 26 clover detectors, each with four sub-detectors with common Compton suppression and 30 tapered single-crystal detectors with individual Compton suppression. In this configuration the total photo-peak efficiency of the array is calculated to be 9.5% [2]. During the early run that produced the data set analysed in this work, however, EUROBALL was still experiencing various kinds of commissioning problems. A total of 14 detectors (one full cluster detector, one full clover detector and three single-crystal detectors) were not mounted. About 15 other crystals had serious resolution or efficiency problems at the beginning of the experiment. Some problems could be corrected during the experiment, but after two days three cluster and two clover detectors were still incomplete and thus running at below their full efficiency. As a result the total photo-peak efficiency is estimated to have been $\lesssim 8.7\%$.

^{143}Eu was populated via the $4n$ exit channel using a beam of ^{37}Cl ions on a stack of three thin (∼0.3 μg/cm^2) ^{110}Pd targets. The beam energy was 160 MeV at the be-

[a] Present address: Division of Cosmic and Subatomic Physics, Lund University, Lund, Sweden

ginning of the experiment and was raised to 165 MeV after two days. Typical "singles" counting rates in the Ge crystals of the cluster, clover and tapered detectors were 4, 6 and 10 kHz, respectively. The event trigger was set to maximise the rate to tape of five-fold coincidences extracted from events with a Compton-suppressed fold $\geqslant 5$. This resulted in a trigger rate of ∼12 kHz and a data rate to tape of about 2 Mbytes/s.

Energy and relative efficiency calibration runs using ^{133}Ba, ^{152}Eu and ^{56}Co sources were performed before, in the middle of and after the five day run.

In the raw Euroball format the data collected occupied 20 DLT Tape IV magnetic tapes or close to 700 Gbytes. The raw data was filtered and compressed off line into a format more suitable for analysis. The "presorted" data, with fold specific data buffers for maximum compression (i.e only one word per 32 kbyte data buffer was needed to specify the clean fold), included for each event two γ-ray energy parameters (ADC range 4 MeV and 20 MeV), unsuppressed fold and a rough γ-ray emission angle classification. The compressed data set occupied only two DLT Tape IV cassettes or ∼70 Gbytes. The presorting also included various filters for "good" events, Compton suppression and pile-up rejection as well as gain, non-linearity and Doppler corrections and the necessary adding of energy signals from scattering between neighbouring crystals of composite detectors. Multiple hits causing more than two signals in the same composite detector were rejected. Two kinds of Doppler correction were employed since it was observed that the finite target thickness induced a spread in the recoil velocity v of the γ-ray emitting nucleus. While the transitions associated with decay of states at lower spin and "normal" deformation occurred at a fixed recoil velocity v the γ rays from superdeformed states were emitted at a changing v corresponding to emission while the recoiling residual nucleus was still slowing down inside the target. Accordingly, for analysis of normally deformed states a fixed v of $0.02215{\cdot}c$ was used for Doppler correction, while for analysis of the superdeformed bands a recoil velocity increasing linearly with E_γ was used instead. This improved the resolution of peaks from the yrast superdeformed band by almost 3 keV or ∼25% at ∼1500 keV.

The cleaned data set used in the analysis contained $4.3{\cdot}10^8$ three-fold, $6.4{\cdot}10^8$ four-fold and $6.8{\cdot}10^8$ five-fold events and $1.0{\cdot}10^9$ events of fold six and higher. The total number of events of all folds was $3.1{\cdot}10^9$, with a mean fold of 4.9.

3 Analysis

The data was sorted into one, two and three-dimensional histograms, with care taken to avoid the "spiking" problem associated with the usage of high-fold coincidences in lower-dimensional histograms [3]. The various analysis programmes of the *Radware* package [4] were then used to view and set gates on the data. The multi-dimensional analysis was supplemented by direct event-by-event sorting when the production of statistically correct one dimensional spectra was crucial or when higher than two-fold gating was desired. For this purpose a small (400 Mbyte) sub-set of the data containing all events satisfying a triple coincidence requirement with the ^{143}Eu yrast superdeformed band and some other especially interesting event classes was stored on hard disk for fast access [5].

In order to enhance long regular correlated rotational cascades the method of *rotational plane mapping* [6,7] was employed in three and four dimensions. In the latter case four-fold and higher coincidences were sorted event-by-event into a two dimensional (2D) matrix of ($E_{\gamma1}$,$E_{\gamma4}$) pairs each representing an energy ordered quadruple coincidence ($E_{\gamma1}$,$E_{\gamma2}$,$E_{\gamma3}$,$E_{\gamma4}$) which satisfied the following "4D rotational plane" relations [7]:

$$N \cdot (E_{\gamma4} - E_{\gamma1}) = (N+2) \cdot (E_{\gamma3} - E_{\gamma2}) \quad (1)$$

$$E_{\gamma1} + E_{\gamma4} = E_{\gamma2} + E_{\gamma3} \quad (2)$$

For a pure rotational spectrum and a given N ($N = 1, 2, 3, ...$) equation 1 selects quadruple coincidences where

- the coincidence ($E_{\gamma1}$,$E_{\gamma4}$) between the smallest and the largest γ-ray energy belongs to one of the 2D rotational ridge numbers $i = j{\cdot}(N+2)$ ($j = 1, 2, 3, ...$),
- given the 2D rotational ridge number i of the ($E_{\gamma1}$,$E_{\gamma4}$) coincidence, the "middle" coincidence ($E_{\gamma2}$,$E_{\gamma3}$) belongs to 2D ridge number $i{\cdot}N/(N+2)$.

Equation 2 further tightens the "regular rotation" requirement.

Requirements 1 and 2 together are extremely selective of regular rotational structures and this method proved very efficient in suppressing the background contributed by the low-lying level structure of ^{143}Eu, which is nearly spherical and dominated by non-rotational multi-particle multi-hole excitations.

Following the method proposed in [8] to identify two-step decay out of superdeformed bands, spectra of all sums of two γ-ray energies in multiple coincidence with the ^{143}Eu yrast superdeformed band were produced. It was also attempted by various methods to locate structures corresponding to constant sums of three γ-ray energies in coincidence with the band.

4 Results

4.1 Superdeformed bands

The E_γ-E_γ-E_γ "cubes" were scanned for superdeformed rotational cascades using the SD search routines in the *Radware* package. Besides the known yrast band in ^{143}Eu, several bands in neighbouring nuclei were identified. These included the bands reported in ^{144}Eu [9,10], ^{142}Eu [10] and ^{142}Sm [11,12]. In the 4D rotational plane matrix shown in Fig. 1 the third SD rotational ridge clearly displays discrete coincidences of the type $[E_\gamma(I), E_\gamma(I+6)], [E_\gamma(I+6), E_\gamma(I+12)]$ etc. Close inspection of the peaks along this ridge yielded the transition energies of a previously unknown superdeformed band. This band is almost isospectral with the more intense ^{143}Eu yrast superdeformed

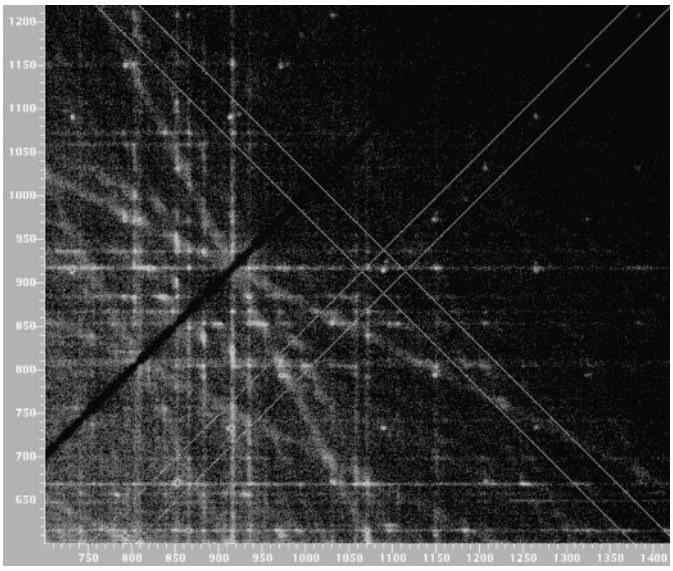

Fig. 1. $N = 1$ 4D rotational plane. The third SD rotational ridge is enclosed by diagonal markers running parallel to the main diagonal. In the center of the cross formed by the two sets of diagonal markers is a 2D peak "representing" the yrast SD band quadruple coincidence $(E_{\gamma 1}, E_{\gamma 2}, E_{\gamma 3}, E_{\gamma 4}) = (913, 972, 1031, 1090)$ keV. This peak and the neighbouring ones along the ridge have small satellites representing cascades in the excited SD band; in the case of the marked peak the satellite represents the cascade $(E_{\gamma 1}, E_{\gamma 2}, E_{\gamma 3}, E_{\gamma 4}) = (924, 980, 1036, 1093)$ keV. Note that this matrix was produced using the conditions of equations 1 and 2 only, i.e. it is neither gated on any SD band nor background-subtracted

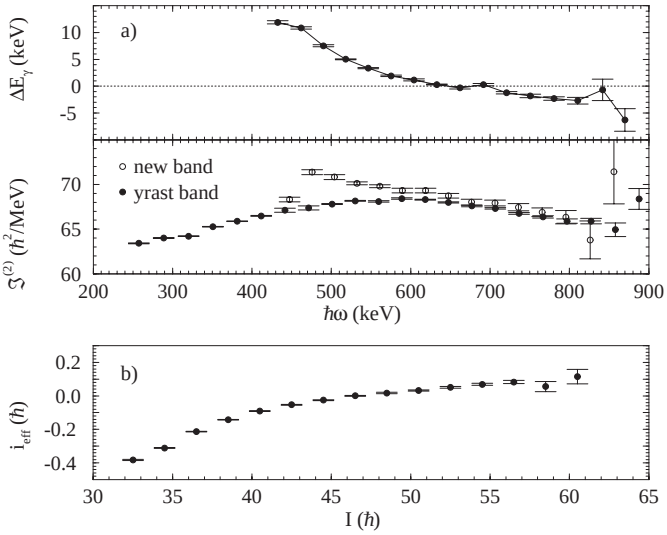

Fig. 2. *a*) Differences in closest transition energies $\Delta E_\gamma = E_\gamma^{new} - E_\gamma^{old}$ (*top*), dynamical moments of inertia $\Im^{(2)}$ (*bottom*). *b*) Effective alignment i_{eff} of the new band relative to the yrast band. The effective alignment plot assumes the spin of the lowest level I_0=30.5 $\hbar$ for the new band

band as is shown in the plot of energy differences between closest transitions in the upper part of Fig. 2a. The transition energies differ significantly only in the lowest 4–5 of the identified transitions, requiring careful selection of non-overlapping gates to produce double and triple coincidence spectra. Background-subtracted triple-gated spectra comparing the new band and the ^{143}Eu yrast band are shown in Fig. 3. The lower lying transitions in the ^{143}Eu yrast band are completely absent in the new band spectrum, indicating the clean separation of the two bands. The transition energies of the new band are given in Table 1 and compared to the ^{143}Eu yrast band in Fig. 2a.

Figure 4 shows the low energy part of the spectrum double gated on selected transitions in the new band. Nearly all strong transitions seen in coincidence with the new band connect states in the spherical part of the low-lying ^{143}Eu level scheme [13]. Assignment of the new band to ^{143}Eu is further supported by the fact that it is clearly seen in a double-gated spectrum produced using the *Radware* programme *Levit8r* on an E_γ-E_γ-E_γ "cube" gated on strong low-lying states in this nucleus. Superdeformed bands belonging to other nuclei seen clearly in the ungated "cube" are not seen in the ^{143}Eu-gated "cube".

The closeness of the transition energies of the new band and the ^{143}Eu yrast band also complicated the determination of the relative transition intensities in the new band. Figure 5 shows the intensity curve extracted

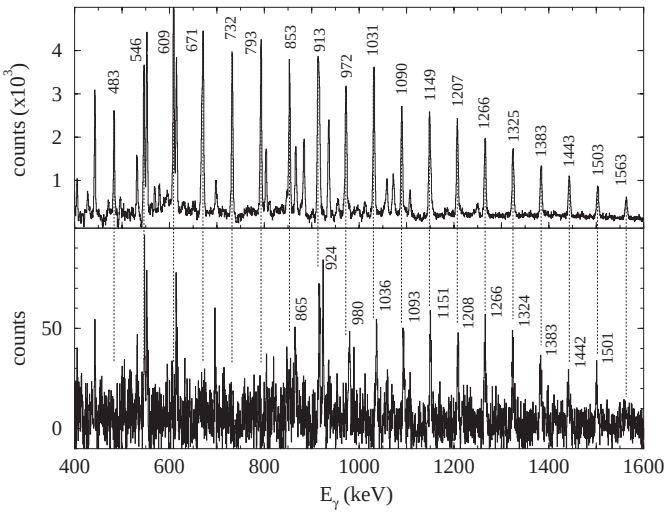

Fig. 3. Spectra in coincidence with clean triple gates on the ^{143}Eu yrast superdeformed band (top) and on the new band (bottom). A fraction of double-gated spectra from the same gate lists have been subtracted as background. The large difference in intensity is mostly due to the fact that only very few gating transitions could be used to obtain a clean spectrum of the new band

from a sum of double gates on three transitions (980 keV, 1036 keV and 1093 keV). Higher-lying transition energies are too close to the yrast band transition energies to allow separation of the two bands. The points in Fig. 5 are normalized to one in the "flat" region of the yrast band intensity curve as determined in the same way (gating on 972 keV, 1031 keV and 1090 keV). This curve is also shown for reference, but has been more accurately determined by other methods elsewhere [8,14]. Detailed comparison of the intensities in the 970–1100 keV interval, which is

Table 1. Transition energies of the superdeformed bands in ^{143}Eu. The error estimates are statistical only. The systematic errors in transition energies are roughly estimated as $\sigma_{syst} \lesssim 0.1$ keV for $E_\gamma \lesssim 1000$ keV, $\sigma_{syst} \lesssim 0.2$ keV for $E_\gamma \lesssim 1600$ keV and $\sigma_{syst} \lesssim 1$ keV for $E_\gamma \gtrsim 1600$ keV. Some transition energies likely to contain larger systematic errors due to close-lying contaminants are marked with asterisks

	$E_{\gamma,new}$ (keV)		$E_{\gamma,yrast}$(keV)
		1	483.28(3)
		2	*546.36(3)
		3	608.85(2)
		4	*671.14(2)
		5	732.42(2)
		6	793.13(2)
1	*865.2(3)	7	853.30(3)
2	923.76(9)	9	*912.9(2)
3	979.8(2)	10	972.26(3)
4	1036.27(8)	11	1031.25(2)
5	1093.3(1)	12	1089.93(3)
6	*1150.6(1)	13	*1148.67(6)
7	1208.3(2)	14	1207.13(3)
8	1266.0(1)	15	1265.69(3)
9	1324.2(2)	16	1324.52(4)
10	1383.0(2)	17	1382.70(5)
11	1441.9(2)	18	1443.12(6)
12	1501.2(3)	19	1503.03(7)
13	1561.0(3)	20	1563.3(1)
14	1621.3(6)	21	1624.0(2)
15	1684(2)	22	1684.7(2)
16	1740(2)	23	1746.3(7)
		24	1804.8(7)

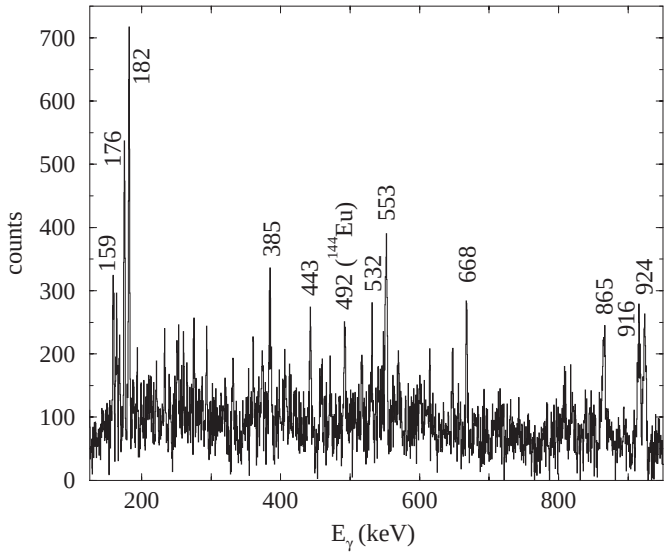

Fig. 4. Low-energy part of spectrum in double coincidence with the three transitions 980 keV, 1036 keV and 1093 keV in the new band. A background double-gated from "background" channels surrounding these transitions has been subtracted

in the "flat", maximum-intensity region for both bands, yields a relative intensity for the new band of 35(4)% of the SD yrast band intensity. The maximum intensity of

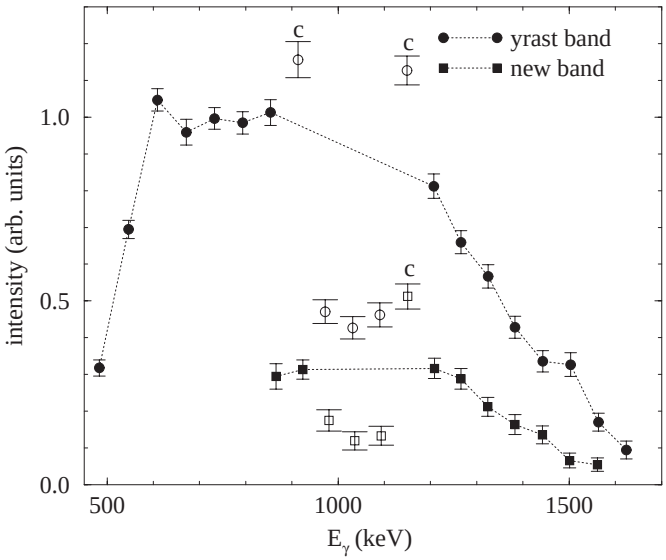

Fig. 5. Intensities of transitions in the ^{143}Eu SD bands. Transitions used for gating and some especially contaminated transitions are included as unfilled points

the yrast band corresponds to 1.8% of the total yield of ^{143}Eu [14].

The dynamical moments of inertia $\Im^{(2)}$ of the two bands are displayed in the lower panel of Fig. 2a. The *fractional change (FC)* [15] is derived from the moments of inertia and is a convenient measure of the degree of similarity between "identical" SD bands, where absolute spins generally are not known. It is defined as the relative difference of the moments of inertia of two bands A and B at a fixed rotational frequency ω:

$$FC = (\Im^{(2)}_A(\omega) - \Im^{(2)}_B(\omega))/(\Im^{(2)}_A(\omega) = di_{eff}/dI_A \quad (3)$$

where the "effective alignment" i_{eff} [15] is defined as

$$i_{eff} = (I_A(\omega) - I_B(\omega))(mod1) \quad (4)$$

The fractional change has been used in several recent theoretical and experimental investigations of the identical band phenomenon [16,17]. If the effective alignment i_{eff} is a linear function of the angular momentum I the *average fractional change* $\overline{FC}$ can be extracted by a linear fit. Figure 2b shows the effective alignment i_{eff} of the new band relative to the yrast band. To get an acceptable linear fit of i_{eff} to I the lowest six data points must be excluded, and the result is an average fractional change $\overline{FC}$ of 0.91(4)% (reduced $\chi^2 = 1.1$). Excluding only the lowest five or the lowest four points results in $\overline{FC}$ values of 1.00(3)% (reduced $\chi^2 = 2.5$) or 1.19(2)% (reduced $\chi^2 = 9.4$) respectively. For comparison with the survey of [16] (see below) the $\overline{FC}$ extracted without regard to the uncertainties in the individual data points is 1.5(2)% using all points (sample standard deviation $\sigma = 0.058$) and 1.4(2)% using all but the lowest point ($\sigma = 0.047$). Excluding the six lowest points this method yields an $\overline{FC}$ of 0.7(1)% ($\sigma = 0.015$).

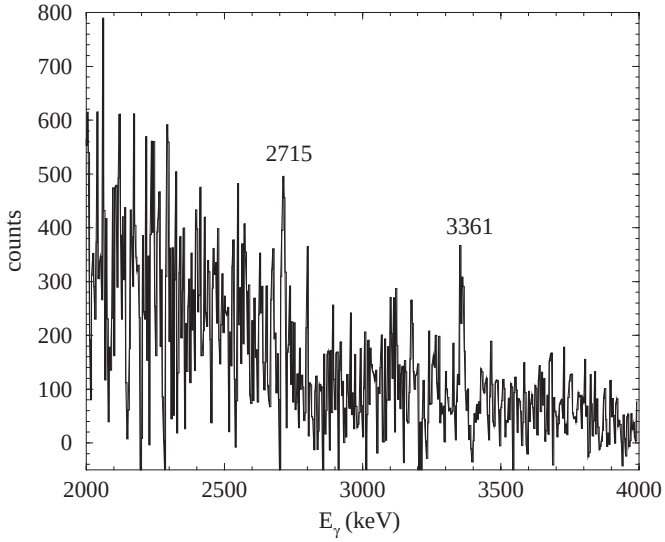

Fig. 6. High-energy part of spectrum in triple coincidence with the yrast SD band, background-subtracted according to the method of [18]

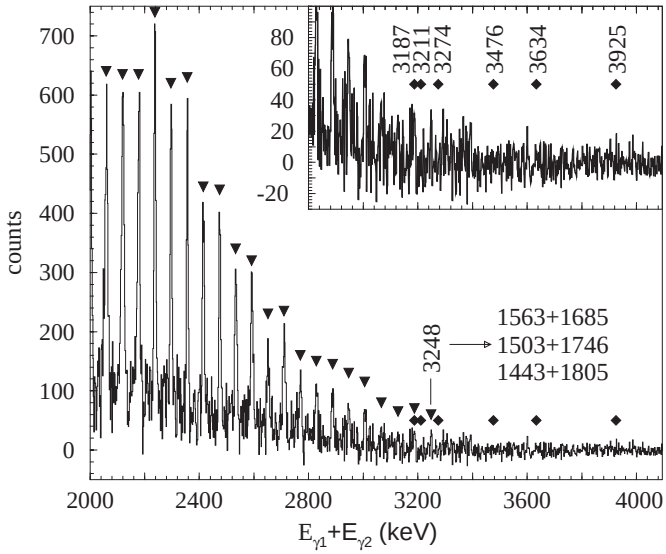

Fig. 7. Spectrum of γ-ray energy sums $E_{\gamma1} + E_{\gamma2}$ in coincidence with four or more yrast SD band transitions and with a difference $|E_{\gamma1} - E_{\gamma2}| < 1$ MeV. A fraction of the triple-gated sum spectrum has been subtracted as background. Sums of transition energies from the yrast SD band appearing above a 2 σ limit are marked with triangles. For the highest SD band sum energy seen above 2 σ, at 3248 keV, the three pairs of known band transitions that result in this sum are given. The diamonds indicate the positions of the sum peaks reported in [8]

4.2 Search for decay-out of SD bands

Attempts were made to identify the decay out of the ^{143}Eu yrast superdeformed band via single- or multi-step transitions to near-yrast normally deformed states.

The 3361 keV transition reported in [19–21] was seen with a significance of $\sim$5.3 σ. It was not possible to connect this transition to the known normally deformed level scheme. Another discrete line at 2715 keV in coincidence with the yrast SD band was also seen with a significance of $\sim$4.7 σ. Figure 6 shows the high-energy part of a triple-gated, background-subtracted spectrum containing the peaks corresponding to the 2715 keV and 3361 keV transitions. The 2715 keV line has an intensity approximately equal to the 3361 keV transition, i.e. about 3% of the full intensity of the yrast SD band. However, it lies in a region of the γ-ray spectrum which has much more continuum background and spectra gated on it have correspondingly much worse peak-to-background ratio. It appears to be in coincidence with all the yrast SD transitions including the lowest known one at 483 keV which is not seen in coincidence with the 3361 keV transition.

Figure 7 shows a spectrum of γ-ray energy sums $E_{\gamma1} + E_{\gamma2}$ in quadruple coincidence with the yrast SD band. It was not possible to confirm the two-step sum peaks first reported in [8]. The absence of satisfactory confirmation of these sum peaks by this and other experiments, despite the significant improvement in statistics with Eurogam and Gammasphere [19,21] suggests that it may be necessary to sum three or more γ rays in order to establish a connection to known normally deformed levels. The background from discrete superdeformed transitions and associated Compton events in various kinds of triple-sum spectra have so far prevented the success of such an analysis.

5 Cranking calculations

Cranked shell model calculations were performed in a mesh surrounding the superdeformed minimum of ^{143}Eu using the *Ultimate Cranker* code [22,23] and modified oscillator potential parameters κ and μ from [24]. The proton and neutron pair gaps $\Delta_{p,n}$ were both fixed at 0.75 MeV, motivated by BCS calculations at cranking frequency $\hbar\omega = 0$ MeV for each $(\epsilon_2, \gamma, \epsilon_4)$ deformation mesh-point. These showed the proton pair gap Δ_p to be almost constant at around 1 MeV throughout the mesh and the neutron pair gap Δ_n to drop with the quadrupole deformation from $\sim$1 MeV at $\epsilon_2 = 0.425$ to $\sim$0.5 MeV at $\epsilon_2 = 0.525$. One- and three-quasiparticle excitations reduce the pairing strength and were expected to occur primarily in the proton system due to the large neutron number N = 80 shell gap. Allowing for this effect the simplifying choice of constant $\Delta_p = \Delta_n = 0.75$ MeV appeared reasonable. Particle number projection was used to ensure that the correct neutron and proton numbers were reproduced, reducing the sensitivity of the results to the Fermi level energy λ. The Fermi level was therefore not determined self-consistently but fixed at the value obtained from a BCS calculation for the vacuum configuration at $\hbar\omega = 0$ MeV. The total energy of the yrast configurations within each of the sixteen symmetry groups defined by all combinations of parity and signature, specified separately in the neutron and in the proton system, were calculated in a frequency range large enough for generation of all angular momenta of interest. Due to the large shell gap at

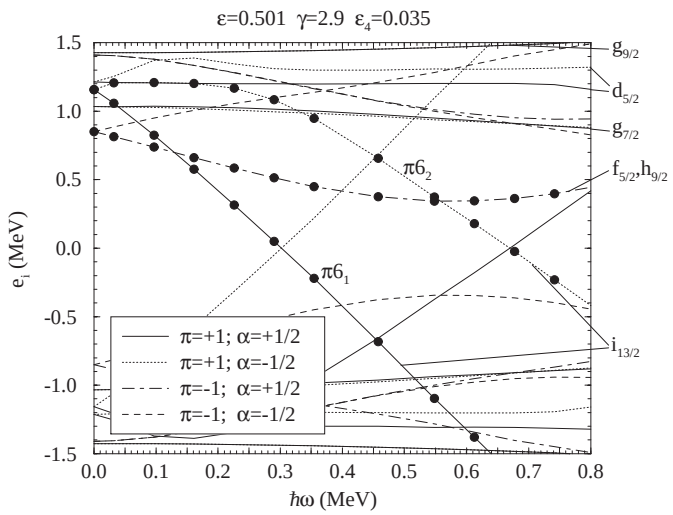

Fig. 8. Proton quasi-particle Routhians at a deformation representative of the SD minimum around $I \sim 40\ \hbar$. The dominant components of the wave functions at low frequency (in the "spherical" Nlj basis) are given on the right for some orbitals of particular interest. The three quasi-proton configuration shown by the filled circles is the $\pi 6^2\ (\pi, \alpha) = (-1, +1/2)$ configuration proposed to be the one on which the new band is based

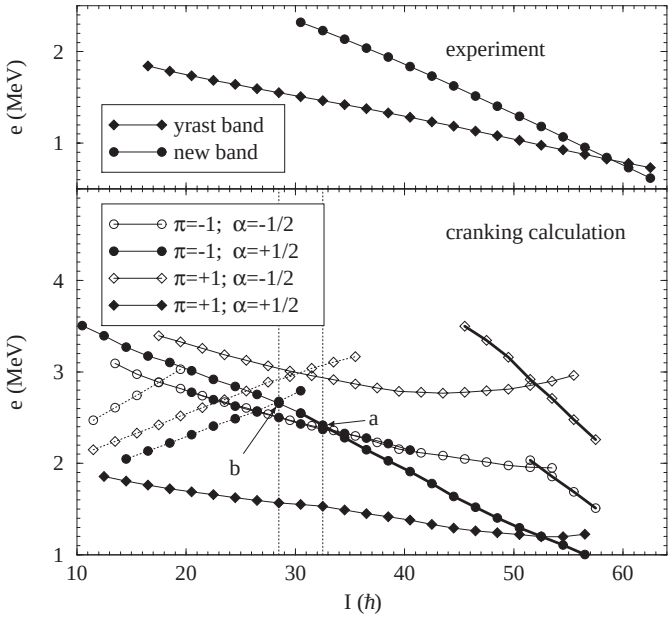

Fig. 9. Total energy $e = E_{tot} - \frac{\hbar^2}{2 \cdot \Im_{rig}} I(I+1)$ for the two experimental bands (upper panel) and in the SD minimum of the deformation mesh for the four yrast configurations given by cranking calculations (lower panel). A rigid rotor reference having $\Im = 66.9\ \hbar^2/\text{MeV}$ has been subtracted to enhance deviations from rigid rotor behaviour. The band head excitation energies of the experimental bands have been arbitrarily set to convenient values. In the lower panel the thickness of the connecting lines indicates the number of proton $i_{13/2}$ intruder orbitals occupied: two for thick lines, one for thin lines and none for dotted lines. The arrows mark the positions of crossings between the $\pi 6^2\ (-1, +1/2)$ configuration and $(\pi, \alpha) = (-1, +1/2)$ configurations with fewer intruder proton orbitals occupied. In the $\pi 6^2\ (-1, +1/2)$ configuration shown in Fig. 8 the indicated crossings occur at $\hbar\omega = 0.44$ MeV (a) and $\hbar\omega = 0.38$ MeV (b)

N = 80 for SD shapes none of the bands competing for yrast position involved any neutron excitations. The total parity π and signature α of these bands were therefore determined by the (π,α) quantum numbers in the proton system with the 80 neutrons contributing a constant $(\pi, \alpha) = (+1, 0)$.

All configurations of interest involve quasi-proton excitations into one or both of the $N = 6$ $i_{13/2}$ intruder orbitals, labelled $\pi 6_{1,2}$ in the sample proton Routhian plot in Fig. 8. In superdeformed ^{143}Eu the position of the $i_{13/2}$ quasi-proton orbitals relative to the Fermi surface results in almost pure particle character for these orbitals. We shall therefore follow the usual convention for non-paired calculations and refer to a configuration involving m $(m = 0, 1, 2, ...)$ quasi-protons in $N = 6$ intruder orbitals as $\pi 6^m$. As stated above the lowest neutron high-N intruder orbitals with $N = 7$ are not populated and the neutron high-N configuration is thus always $\nu 7^0$. Other positive parity proton orbitals near the Fermi surface are dominated by $N = 4$ $g_{7/2}$, $g_{9/2}$ and $d_{5/2}$ components while the negative parity orbitals involve mostly $h_{9/2}$, $h_{11/2}$, $f_{5/2}$ and $f_{7/2}$ components from the $N = 5$ oscillator shell.

The upper panel of Fig. 9 shows the excitation energies of the experimental bands as a function of total angular momentum and relative to a "convenient" rigid rotor reference. The plot assumes for the yrast band the spin of the lowest level $I_0 = 16.5\ \hbar$ as suggested in [25] and for the new band $I_0 = 30.5\ \hbar$. The lower panel shows the interpolated total energy of the SD minimum for the lowest-lying calculated configurations with given parity and signature relative to the same rigid rotor reference. For the calculated bands the Fig. illustrates how the yrast configuration in each (π, α) symmetry group changes from involving no $N = 6$ proton intruder orbitals at low angular momentum to involving one and finally two intruder protons. The positions of the interpolated SD minima for the four configurations which are yrast in the $I \simeq 30$–$50\ \hbar$ region are shown in Fig. 10 in terms of the $(\epsilon_2, \gamma, \epsilon_4)$ deformation parameters. The ϵ_2 deformation of the $\pi 6^2\ (\pi, \alpha) = (-1, +1/2)$ configuration (dash-dotted line) is reduced relative to the other configurations for angular momentum $I \lesssim 30\ \hbar$. This is due to a strong interaction where the second-most aligned $N = 6$ proton intruder orbital $(\pi 6_2)$ exchanges its character with a predominantly $d_{5/2}$ $N = 4$ orbital. The effect is also seen in Fig. 9, where the band represented at high angular momentum by filled circles connected by thick lines continues into an yrare $\pi 6^1\ (-1, +1/2)$ configuration at low angular momentum. As seen in Fig. 9 this change in the $\pi 6^2\ (\pi, \alpha) = (-1, +1/2)$ configuration occurs below the crossing with the $\pi 6^1\ (-1, +1/2)$ configuration at $\hbar\omega \simeq 0.44$ MeV.

The total angular momentum relative to the rigid rotor reference is displayed as a function of rotational frequency

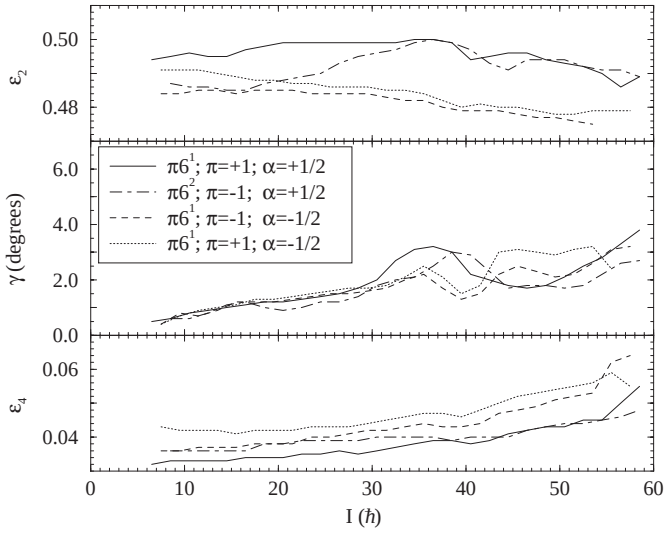

Fig. 10. Deformation parameters of the SD minimum for the four configurations calculated to be yrast in the $I \simeq 30$–$50\ \hbar$ region

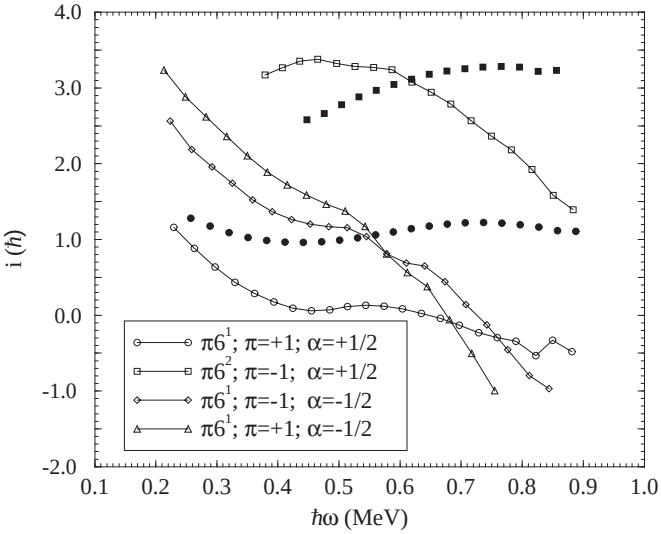

Fig. 11. Angular momentum $i = I - \Im \cdot \omega$ relative to a rigid rotor having $\Im = 66.9\ \hbar^2$/MeV for the two experimental SD bands compared with cranking calculations for the same low-lying configurations as in figure 9. The experimental bands are represented by filled circles (yrast band) and filled squares (new band) and the calculated bands by open symbols

in Fig. 11 for the four configurations $\pi 6^1\ (+1,+1/2)$, $\pi 6^1\ (+1,-1/2)$, $\pi 6^2\ (-1,+1/2)$ and $\pi 6^1\ (-1,-1/2)$. Also shown are the same quantities for the experimental bands with the same spin assumptions as for Fig. 9. For all the calculated bands Fig. 11 shows a reduction in angular momentum with rotational frequency relative to experimental data. With a smaller constant pair gap parameter in the cranking calculation this discrepancy is reduced, indicating that it is an effect of not treating pairing self consistently. This explanation is consistent with the fact that the three-quasiparticle configurations $\pi 6^1\ (+1,-1/2)$, $\pi 6^2\ (-1,+1/2)$ and $\pi 6^1\ (-1,-1/2)$ are most strongly affected. A thorough investigation on the inclusion of self-consistent pairing in cranking calculations for SD nuclei is currently being performed [26].

In a recent study [27] a slightly different set of Nilsson potential parameters κ and μ was used in order to provide a better description of SD bands in the whole mass A$\sim$130–150 region. The effect of using these parameters instead of the "standard" set [24] was investigated. This calculation was carried out for the interesting configurations at the deformation of the SD minimum at I=34.5 $\hbar$ as determined from the mesh calculation. The main effect in the proton system was to change the character of the wave-function of the $N = 4$, $\alpha = -1/2$ orbital crossing the $\pi 6_2$ orbital at $\hbar\omega \simeq 0.35$ MeV (see Fig. 8) from one dominated by a $g_{7/2}$ component to one dominated by a $d_{5/2}$ component. The total energy of all configurations involving this $N = 4$ orbital was raised slightly but the $\pi 6^1/\pi 6^2$ crossing frequencies seen in the total energy plot of Fig. 9 were not significantly affected. Unfortunately the strong interaction between the $d_{5/2}$-dominated orbital and the $\pi 6_2$ orbital crossing it makes a full mesh calculation for deformation self-consistent treatment of the interesting configurations using the modified oscillator parameters of [27] very difficult. With the parameters of [24] the $\pi 6^1/\pi 6^2$ crossing involves the $N = 4$ $g_{7/2}$-dominated orbital instead, with a weaker interaction at the crossing. The $g_{7/2}$ and $d_{5/2}$ orbitals in question are, however, "pseudo-spin" partners and therefore can be expected to have approximately the same deformation-driving properties. The alignment of the $N = 4$ mixed $g_{7/2}/d_{5/2}$ orbital is also approximately the same whether it is dominated by the $g_{7/2}$ or $d_{5/2}$ component.

6 Discussion

The intensity profiles displayed in Fig. 5 show that the decay-out of the SD minimum proceeds differently from the new band compared to the yrast band. In the former case the last transition is seen with the full intensity of the "flat top" region while in the latter case the SD band loses its intensity more gradually over the three lowest states. An explanation for this behaviour is suggested by the cranking calculations, which show that a $\pi 6^2$, $(\pi,\alpha) = (-1,+1/2)$ band is crossed by a $(-1,+1/2)$ band with only one $i_{13/2}$ intruder orbital occupied at the frequency $\hbar\omega \simeq 0.44$ MeV. This is very close to the frequency of the lowest observed transition in the new band, $\hbar\omega \simeq E_\gamma/2 \simeq 0.43$ MeV. Identification of the $\pi 6^2$ configuration with the new SD band also makes it reasonable that it should be rather intensely populated relative to the yrast band, presumably the $\pi 6^1\ (+1,+1/2)$ band seen in Fig. 9: the two bands compete for the yrast position in the high-spin feeding region around $I\sim$50 $\hbar$.

Despite the close agreement of the calculated $\pi 6^2/\pi 6^1$ crossing frequency with the apparent decay-out frequency one can imagine other configuration assignments for the new band. One possibility suggested by Fig. 9 is the $\pi 6^1$ configuration in the $(\pi,\alpha) = (-1,+1/2)$ symmetry group.

The two almost degenerate $\pi 6^1$ configurations represented by circles and thin solid lines in Fig. 9 are identical three-quasiparticle excitations except for the inclusion of different members of a predominantly $g_{7/2}$ $N = 4$ signature partner pair. If the new band in fact corresponds to the $\alpha = +1/2$ member of this pair one might also expect sudden decay-out due to the structural change as this $\pi 6^1$ band is crossed by a $\pi 6^0$ band at slightly lower spin (and frequency) compared to the $\pi 6^2/\pi 6^1$ crossing mentioned above. This interpretation has the disadvantage of predicting decay out at lower frequency than the experimentally observed one. With such a configuration for the new band one would also expect to see the $\alpha = -1/2$ signature partner but this is not the case. On the other hand the $\pi 6^1$ assignment has the advantage of basing the two very similar bands in ^{143}Eu on the same single proton high-N intruder orbital. It should be pointed out that the agreement in alignment between experiment and calculations is not improved by the above alternative assignment: the $\pi 6^1$, $\alpha = -1/2$ member of the signature partner pair is represented by open triangles in Fig. 11.

It is difficult to assess which degree of similarity in dynamical moments of inertia and/or transition energies justifies the label "identical" for this pair of SD bands. The common practice of expressing a criterion relative to the change expected due to the effect of a mass difference on the "rigid rotor" moment of inertia (proportional to $A^{5/3}$), employed for example in the survey of [16], is not directly applicable. In order to make a comparison with this study one could disregard the absence of a mass difference on the assumption that the influence of a small mass difference on the moment of inertia of a superdeformed nucleus should in any case be considerably less important than the properties of the specific orbitals occupied in each configuration [17]. Thus comparing with the results of [16] the average fractional change $\overline{FC}$ in the "identical" region of 0.91(4)% is somewhat smaller than the $\overline{FC} \gtrsim 2\%$, which would be expected if the configurations differ by one high-N intruder proton. In [16], however, error limits were not assigned to the transition energies of the pairs of bands examined and the criterion for an acceptable linear fit was one that gave a sample standard deviation $\sigma < 0.05$. Including all i_{eff} data points but one in a fit and disregarding the error limits on the individual points for the pair of bands in ^{143}Eu results in an average fractional change of 1.4(2)% with $\sigma = 0.047$.

In [17] the distribution of the fractional change FC in $\mathcal{J}^{(2)}$ for pairs of bands from low-lying configurations in SD ^{152}Dy as obtained from cranking calculations was studied. It was found that there is a correlation between the high-N intruder orbital content and the centroid of the FC distribution, so that the FC distribution for pairs of bands with the same number of $N = 6$ protons is centered on $FC = 0$ while for pairs of bands differing by one intruder proton the distribution is centered on $FC \simeq 2\%$. The width of both distributions, however, is approximately 10%, which means that an average fractional change of 0.91% is compatible both with the bands having the same number of $N = 6$ intruder protons and with a difference of one intruder proton.

We propose as the most likely configuration for the new band the $\pi 6^2$ ($\pi = -1, \alpha = +1/2$) three quasi-proton excitation shown in Fig. 8, differing from the one quasi-proton $\pi 6^1$ ($\pi = +1, \alpha = +1/2$) yrast configuration by one high-N intruder proton.

7 Summary

In conclusion, a new superdeformed band has been found in ^{143}Eu with transition energies very close to those of the previously known yrast band. The new band retains its maximum intensity of 35% compared to the yrast band down to the lowest observed transition. An explanation for this "sudden" decay out is suggested by cranked shell model calculations, which show a band crossing at approximately the observed decay out frequency. This interpretation implies that the new band is based on a configuration involving two $N = 6$ intruder protons and that it has the parity and signature quantum numbers $(\pi, \alpha) = (-1, +1/2)$. The calculated excitation energy of the $\pi 6^2$ $(-1, +1/2)$ configuration relative to the yrast band lends further support to this configuration assignment.

A new discrete line at 2715 keV in coincidence with the yrast SD band was found, but it was not possible to connect the SD bands to known normally deformed states.

We would like to thank Ragnar Bengtsson for advice on cranking calculations and for helpful and stimulating discussions. The skillful operation of the Legnaro Tandem-ALPI accelerator by the L.N.L technical staff is gratefully acknowledged. This work was funded by the Swedish and Danish Natural Science Research Councils.

References

1. S. Leoni et al., Phys. Lett. B **353**, 179 (1995)
2. J. Simpson, Z. Phys. A **358**, 139 (1997)
3. C.W. Beausang et al., Nucl. Instr. and Meth. in Phys. Research A **364**, 560 (1995)
4. D.C. Radford, Nucl. Instr. and Meth. A **361**, 297 (1995)
5. J. Nyberg et al., TSL Progress Report 1994-1995, 1995 (unpublished)
6. B. Herskind et al., Phys. Lett. B **276**, 4 (1992)
7. P.H. Rasmussen, M.Sc. thesis, The Niels Bohr Institute, University of Copenhagen, 1993
8. A. Ataç et al., Phys. Rev. Lett. **70**, 70 (1993)
9. G. Hackman et al., Phys. Rev. C **55**, 1101 (1997)
10. S.M. Mullins et al., Phys. Rev. C **52**, 99 (1995)
11. G. Hackman et al., Phys. Rev. C **47**, R433 (1993)
12. G. Hackman et al., Phys. Rev. C **52**, R2293 (1995)
13. M. Piiparinen et al., Nucl. Phys. A **605**, 191 (1996)
14. L. Roos, M.Sc. thesis, Uppsala University, 1996
15. C. Baktash et al., Ann. Rev. Nucl. Part. Sci. **45**, 485 (1995)
16. G. de France et al., Phys. Rev. C **53**, R1070 (1996)
17. L. Karlsson et al., Phys. Lett. B **416**, 16 (1998)

18. A. Crowell et al., Nucl. Instr. and Meth. A. **355**, 575 (1995)
19. A. Ataç et al., Z. Phys. A **355**, 343 (1996)
20. A. Axelsson et al., Prog. Part. Nucl. Phys. **38**, 195 (1997)
21. F. Lerma et al., Phys. Rev. C **56**, R1671 (1997)
22. T. Bengtsson, Understanding the Ultimate Cranker – a sort of manual, Lund Institute of Technology, Department of Mathematical Physics report
23. R. Bengtsson. (private communication)
24. T. Bengtsson, I. Ragnarsson, Nucl. Phys. A **436**, 14 (1985)
25. S. Lunardi et al., Nucl. Phys. A **618**, 238 (1997)
26. A. Axelsson et. al. (to be published)
27. L. Karlsson, Ph.D. thesis., Lund Institute of Technology, 1999